(Preprint) AAS 25-665

CONSTANT-DIRECTION OPTIMAL LOW THRUST CONTROL FOR SPACECRAFT RENDEZVOUS HOVERING PHASES

Chuncheng Zhao [*], Michele Maestrini [†], and Pierluigi Di Lizia [‡]

This paper investigates a low-thrust optimal control problem with a constant thrust direction for the spacecraft rendezvous hovering phase. The thrust direction is assumed to be fixed in the local Radial-Transverse-Normal (RTN) frame attached to the active spacecraft. To address this challenge, the energy-optimal control problem is first formulated using RTN-constant thrust in inertial dynamics and then analytically solved via the state transition matrix (STM) method. By adopting a least-squares solution, a favorable constant direction with strong operational performance can be rapidly identified, and its reliability is validated through comparisons with numerical methods. Finally, the fuel-optimal control problem is formulated as a nonlinear programming (NLP) problem and efficiently solved using the selected direction and corresponding energy-optimal solution as the initial guess.

INTRODUCTION

Autonomous spacecraft rendezvous is critically important in near-Earth missions such as on-orbit servicing and active space debris removal.[1] The development of robust and efficient autonomous guidance and control algorithms for these applications has been extensively investigated in recent decades.[2,3] The increasing use of small satellites has further heightened the need for effective and reliable control strategies, particularly given their limited computational resources and actuation capabilities.[4,5] During rendezvous operations, a waiting phase—commonly referred to as relative hovering[6]—may be introduced to allow time for command reception or target information acquisition, while maintaining a safe relative distance.[7,8] This phase has been a focus of research recently.[9]

The concept of relative hovering was initially proposed for station-keeping around small celestial bodies,[10,11] and later extended to near-Earth spacecraft missions. State-of-the-art control methods for relative hovering between two spacecraft generally fall into two main categories: (1) maintaining a fixed relative position with respect to the target in a local rotating reference frame, and (2) tracking a predefined relative trajectory within a bounded zone near the target. For the former, Dang et al.[6] provided a comprehensive survey and further explored the problem including the effects of J_2 perturbations. Furthermore, Huang et al.[12] developed nonlinear control strategies for underactuated satellites using a sliding mode control approach. Regarding the latter approach, Irvin et al.[13] proposed a periodic forced relative orbit, known as the teardrop orbit, geometrically designed under

[*]PhD Candidate, Department of Aerospace Science and Technology, Politecnico di Milano, Via La Masa 34, 20156 Milano, Italy.
[†]Assistant Professor, Department of Aerospace Science and Technology, Politecnico di Milano, Via La Masa 34, 20156 Milano, Italy.
[‡]Associate Professor, Department of Aerospace Science and Technology, Politecnico di Milano, Via La Masa 34, 20156 Milano, Italy.

the assumption of unperturbed orbital dynamics. Maintaining this orbit requires maneuvers once per orbital period, meaning that the relative trajectory's geometry imposes an upper limit on mission duration for a given mass budget. As an alternative, Deaconu et al.[14] derived natural relative orbits that meet both the spatial constraints of a hovering zone and periodicity conditions, using parametric representations of relative motion. These periodic orbits require no control input in the absence of perturbations, thus minimizing fuel consumption. Building on this foundation, Arantes et al.[15] proposed a novel method for representing space-restricted periodic trajectories through polynomial inequalities, offering a simpler and more computationally efficient framework. Based on these periodic orbits, impulsive control strategies have been developed to ensure relative hovering in perturbed environments. For instance, Arantes et al.[16] designed a globally stable controller using a three-impulse sequence, tailored to the set of admissible trajectories. Subsequently, Sanchez et al.[17] introduced an event-triggered control scheme for improved responsiveness and efficiency.

Impulsive maneuvers assume instantaneous thrust, which is an idealization not applicable to realistic spacecraft propulsion systems. A practical alternative is to approximate impulsive thrust using finite-duration continuous thrust.[18] The growing use of small satellites, such as CubeSats, introduces additional challenges due to their limited actuation capabilities and typically low thrust levels. Moreover, the increasing adoption of electric propulsion in modern space missions highlights the potential of low-thrust control, particularly for micro-satellite applications.[19] To support long-term hovering, a low-thrust optimal control strategy has been investigated.[20] However, this study employed a tangential thrust, which is restricted to in-plane motion control. Consequently, the development of efficient low-thrust control schemes remains an active area of research.

The work presented in Reference 20 is limited to in-plane motion control due to its use of purely tangential thrust. However, many mission scenarios require full six-degree-of-freedom (6-DOF) orbital control, which presents a significant challenge for underactuated spacecraft. This paper extends prior research by designing an optimal low-thrust control scheme that enables full 6-DOF maneuvering using a constant thrust direction defined in the local RTN frame. First, the active spacecraft's inertial dynamics are formulated with a control input whose direction is fixed in the RTN frame. A series of energy-optimal control problems with fixed RTN directions are then analytically solved using the inertial STM method, similar to the approach in References 20, 21. A least-square approach is employed to select the most favorable thrust directions based on control performance, and the effectiveness of this method is validated through comparisons with numerical techniques. Finally, using the identified constant thrust direction and an initial nominal firing window, the fuel-optimal control problem is formulated as a NLP problem. The resulting solution yields both the optimal bang-bang thrust profile and the corresponding RTN-constant direction.

This paper is organized as follows. First, the formulation of the energy-optimal control problem with a RTN-constant thrust direction is presented, along with its analytical solution using the inertial STM. Next, the procedure for formulating the corresponding fuel-optimal control problem as a NLP is introduced. Finally, a simulation case of relative hovering is provided to validate the effectiveness of the proposed method.

LOW THRUST CONTROL DESIGN

The orbital motion of two spacecraft is illustrated in Figure 1(a). The active spacecraft performing the relative hovering maneuver is referred to as the follower, while the passive spacecraft, serving as the mission target, is designated as the leader. The Earth-Centered Inertial (ECI) frame is defined by $O, \boldsymbol{I}, \boldsymbol{J}, \boldsymbol{K}$, and the follower's motion is described in this frame for the purpose of designing the optimal low-thrust control strategy. To characterize relative motion, a Local Vertical/Local Horizontal (LVLH) frame is established at the mass center of the leader spacecraft S_l, denoted by $S_l, \boldsymbol{i}, \boldsymbol{j}, \boldsymbol{k}$. In this frame, $\boldsymbol{k}$ is the radial unit vector pointing toward the Earth's center (O), $\boldsymbol{j}$ is the cross-track unit vector pointing opposite to the orbital angular momentum, and $\boldsymbol{i}$ is the along-track unit vector, completing a right-handed coordinate system. The relative position vector $\boldsymbol{\rho}$ of the follower S_f is expressed in the LVLH frame, while $\boldsymbol{r}_f$ and $\boldsymbol{r}_l$ represent the inertial positions of the follower and leader, respectively, in the ECI frame. Additionally, a RTN frame is defined at the follower to specify the constant thrust direction. In this frame, the radial axis aligns with the position vector $\boldsymbol{r}_f$, the normal axis corresponds to the orbital angular momentum vector, and the transverse axis completes the right-handed rule.

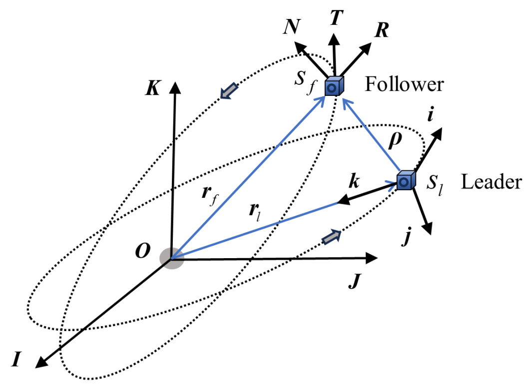

(a) Orbital frames

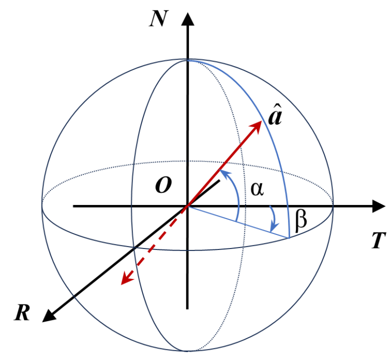

(b) Constant thrust direction

Figure 1. Definition of orbit motion.

The constant thrust direction, denoted as $\hat{\boldsymbol{a}}$ in Figure 1(b), is defined in the RTN frame by two constant angles, α and β, so that $\hat{\boldsymbol{a}} = \cos\alpha\sin\beta\vec{\boldsymbol{R}} + \cos\alpha\cos\beta\vec{\boldsymbol{T}} + \sin\alpha\vec{\boldsymbol{N}}$. The unit vectors $\vec{\boldsymbol{R}}$, $\vec{\boldsymbol{T}}$, and $\vec{\boldsymbol{N}}$ defining the RTN frame are given by, $\vec{\boldsymbol{R}} = \frac{\boldsymbol{r}}{r}$, $\vec{\boldsymbol{T}} = \frac{\boldsymbol{v}}{v}$, and $\vec{\boldsymbol{N}} = \frac{\boldsymbol{h}}{h}$ where $\boldsymbol{h} = \boldsymbol{r} \times \boldsymbol{v}$. In these formulations, the vector is denoted using the bold font, e.g. $\boldsymbol{r}$, and its Euclidean norm is denoted using the normal font e.g. r. Note that the transverse direction is taken as the direction of the velocity vector. This formulation assumes, as an approximation, that the velocity vector remains perpendicular to the position vector, which is reasonable for near-circular orbits. The inertial dynamics of the follower, incorporating a control term in a RTN-constant direction, are expressed as,

$$\begin{cases} \boldsymbol{r} = \dot{\boldsymbol{v}} \\ \dot{\boldsymbol{v}} = -\dfrac{\mu}{r^3}\boldsymbol{r} + a_c(\cos\alpha\sin\beta\vec{\boldsymbol{R}} + \cos\alpha\cos\beta\vec{\boldsymbol{T}} + \sin\alpha\vec{\boldsymbol{N}}) \end{cases} \tag{1}$$

where μ is Earth's gravitational constant, a_c is the magnitude of control acceleration. The vector $\boldsymbol{r}$ and $\boldsymbol{v}$ represent the inertial position and velocity of the follower, omitting the subscript f for simplicity. This study assumes that the variation in spacecraft mass due to fuel consumption is negligible. This assumption is reasonable for close-range proximity operations using low thrust,[20,21] and allows the omission of the mass variation equation, simplifying the formulation of the subsequent optimal control problems. In general, the control requirements of relative hovering are defined in terms of relative states. Once a relative state and a time duration are specified, the corresponding inertial state of the follower can be directly calculated from the leader's inertial state and the definition of LVLH frame.[22]

Energy-Optimal Control

First, the energy-optimal problem is investigated and solved using the inertial STM method. For a specific hovering mission, the boundary conditions can be given as,

$$\begin{cases} \boldsymbol{r}(t_0) = \boldsymbol{r}_0 \\ \boldsymbol{v}(t_0) = \boldsymbol{v}_0 \end{cases} \text{and} \begin{cases} \boldsymbol{r}(t_f) = \boldsymbol{r}_f \\ \boldsymbol{v}(t_f) = \boldsymbol{v}_f \end{cases} \tag{2}$$

where $[\boldsymbol{r}_0; \boldsymbol{v}_0]$ are initial inertial states at initial time t_0, and $[\boldsymbol{r}_f; \boldsymbol{v}_f]$ are target inertial states at final time t_f. Given the constants α and β, the energy-optimal control problem is formulated as,

$$\begin{aligned} &\min \int_{t_0}^{t_f} \frac{1}{2} a_c^2 \mathrm{d}t \\ &\text{st. the dynamics Eq. (1) and boundary conditions Eq. (2).} \end{aligned} \tag{3}$$

From the optimal control theory,[23] the Hamiltonian of this problem is written as,

$$H = \frac{1}{2} a_c^2 + \boldsymbol{\lambda}_r^{\mathrm{T}} \boldsymbol{v} + \boldsymbol{\lambda}_v^{\mathrm{T}} (-\frac{\mu}{r^3} \boldsymbol{r} + a_c \hat{\boldsymbol{a}}) \tag{4}$$

Based on the Pontryagin's minimum principle, the magnitude of optimal control yields,

$$a_c^* = -\left(\cos\alpha \sin\beta \frac{\boldsymbol{r}^{\mathrm{T}} \boldsymbol{\lambda}_v}{r} + \cos\alpha \cos\beta \frac{\boldsymbol{v}^{\mathrm{T}} \boldsymbol{\lambda}_v}{v} + \sin\alpha \frac{\boldsymbol{h}^{\mathrm{T}} \boldsymbol{\lambda}_v}{h} \right) \tag{5}$$

From the Euler-Lagrange equations, the costate dynamics can be obtained as,

$$\begin{cases} \dot{\boldsymbol{\lambda}}_r = \dfrac{\mu}{r^3} \boldsymbol{\lambda}_v - \dfrac{3\mu \boldsymbol{r}\boldsymbol{r}^{\mathrm{T}}}{r^5} \boldsymbol{\lambda}_v - \ldots \\ \qquad a_c^* \left(\cos\alpha \sin\beta \left(\mathbf{I}_{3\times3} - \dfrac{\boldsymbol{r}\boldsymbol{r}^{\mathrm{T}}}{r^2} \right) \dfrac{\boldsymbol{\lambda}_v}{r} + \sin\alpha \left(\mathbf{I}_{3\times3} - \dfrac{\boldsymbol{h}\boldsymbol{h}^{\mathrm{T}}}{h^2} \right) \dfrac{\boldsymbol{v} \times \boldsymbol{\lambda}_v}{h} \right) \\ \dot{\boldsymbol{\lambda}}_v = - \boldsymbol{\lambda}_r - a_c^* \left(\cos\alpha \cos\beta \left(\mathbf{I}_{3\times3} - \dfrac{\boldsymbol{v}\boldsymbol{v}^{\mathrm{T}}}{v^2} \right) \dfrac{\boldsymbol{\lambda}_v}{v} + \sin\alpha \left(\mathbf{I}_{3\times3} - \dfrac{\boldsymbol{h}\boldsymbol{h}^{\mathrm{T}}}{h^2} \right) \dfrac{\boldsymbol{\lambda}_v \times \boldsymbol{r}}{h} \right) \end{cases} \tag{6}$$

Introduce Eq. (5) into the dynamics Eq. (1), and combine states and costate dynamics, this energy optimal problem can be expressed as,

$$\begin{cases} \dot{\boldsymbol{r}} = \boldsymbol{v} \\ \dot{\boldsymbol{v}} = -\dfrac{\mu}{r^3} \boldsymbol{r} + a_c^* \hat{\boldsymbol{a}} \\ \dot{\boldsymbol{\lambda}}_r = \dfrac{\mu}{r^3} \boldsymbol{\lambda}_v - \dfrac{3\mu \boldsymbol{r} \cdot \boldsymbol{\lambda}_v}{r^5} \boldsymbol{r} - a_c^* (\cdots) \\ \dot{\boldsymbol{\lambda}}_v = -\boldsymbol{\lambda}_r - a_c^* (\cdots) \end{cases} \tag{7}$$

It becomes a Two-Point Boundary Value Problem (TPBVP) if the time window $[t_0, t_f]$ and the boundary conditions are given, and it can be transformed into an Initial Value Problem (IVP) aiming at find the initial condition $(\boldsymbol{\lambda}_{r0}, \boldsymbol{\lambda}_{v0}, \alpha, \beta)$ satisfying final boundary conditions. Then, this IVP can be solved by numerical shooting method,

$$\begin{aligned} &\text{Find } (\boldsymbol{\lambda}^*_{r_0}, \boldsymbol{\lambda}^*_{v_0}, \alpha^*, \beta^*), \text{ that } (\boldsymbol{r_f^*}, \boldsymbol{v_f^*}) = f(\boldsymbol{r}_0, \boldsymbol{v}_0, \boldsymbol{\lambda}^*_{r_0}, \boldsymbol{\lambda}^*_{v_0}, \alpha^*, \beta^*) \\ &\text{satisfying } \begin{cases} \boldsymbol{r_f^*} - \boldsymbol{r}_f = \boldsymbol{0} \\ \boldsymbol{v_f^*} - \boldsymbol{v}_f = \boldsymbol{0} \end{cases} \end{aligned} \tag{8}$$

where f represents the integration of Eq. (7) from initial condition $(\boldsymbol{r}_0, \boldsymbol{v}_0, \boldsymbol{\lambda}_{r_0}, \boldsymbol{\lambda}_{v_0}, \alpha, \beta)$ in time duration $[t_0,\ t_f]$. Here, the parameters $(\alpha,\ \beta)$ representing the constant thrust direction are also treated as unknown constants and included in the shooting process as optimization parameters. However, the numerical method is time-consuming and may encounter convergence issues if an inadequate initial guess is used. Given these limitations, also in consideration of the computational capabilities of small satellites, searching for a solution numerically is considered inadequate. Therefore, a faster and more robust approach is needed.

Given the computational efficiency required for solving the above problem, the analytical method based on the STM[20] is preferred. This method is applied to solve the energy-optimal problem, assuming that the thrust direction is known. Consequently, α and β are treated as known constants, allowing the STM to be computed over a specified time interval. To identify beneficial constant thrust directions, a search domain for the angles α and β is defined. Within this domain, a set of energy-optimal problems—each corresponding to a distinct thrust direction—is rapidly solved. The resulting solutions are evaluated to determine the most promising candidate direction for subsequent use in solving the fuel-optimal control problem.

To facilitate this process, Eq. (7) is linearized around the nominal Keplerian dynamics, enabling the computation of an inertial STM $\boldsymbol{\Phi}$ that analytically propagates variations in the initial state and costate. This approximation requires only the integration of basic Keplerian motion and a single STM computation for the desired time interval, thereby significantly reducing computational cost. The STM is derived from the following system of ordinary differential equations,

$$\dot{\boldsymbol{\Phi}}(t, t_0) = \mathbf{J}(t)\boldsymbol{\Phi}(t, t_0), \quad \boldsymbol{\Phi}(t_0, t_0) = \mathbf{I}_{12\times 12} \tag{9}$$

where $\mathbf{J}$ is the Jacobian of the dynamics system expressed in Eq. (7) and evaluated on the nominal Keplerian orbit as,

$$\mathbf{J} = \begin{bmatrix} \mathbf{0}_{3\times3} & \mathbf{I}_{3\times3} & \mathbf{0}_{3\times3} & \mathbf{0}_{3\times3} \\ -\mathbf{J}_{34} & \mathbf{0}_{3\times3} & \mathbf{0}_{3\times3} & \mathbf{J}_{24} \\ \mathbf{0}_{3\times3} & \mathbf{0}_{3\times3} & \mathbf{0}_{3\times3} & \mathbf{J}_{34} \\ \mathbf{0}_{3\times3} & \mathbf{0}_{3\times3} & -\mathbf{I}_{3\times3} & \mathbf{0}_{3\times3} \end{bmatrix}, \tag{10}$$

$$\mathbf{J}_{24} = -\,[\hat{\boldsymbol{a}}\hat{\boldsymbol{a}}^{\mathrm{T}}]_{3\times3},\ \mathbf{J}_{34} = \frac{\mu}{r_n^3}\mathbf{I}_{3\times3} - \frac{3\mu}{r_n^5}[\boldsymbol{r}_n\boldsymbol{r}_n^{\mathrm{T}}]_{3\times3}$$

Here $\boldsymbol{r}_n = [r_{nx}; r_{ny}; r_{nz}]$ represents the inertial position of nominal trajectory and $\mathbf{I}_{n\times n}$ represents the $n \times n$ identity matrix. Thanks to this STM, the variations of initial states are linearly mapped into variations of final states by,

$$[\delta\boldsymbol{r}_f; \delta\boldsymbol{v}_f; \delta\boldsymbol{\lambda}_{r_f}; \delta\boldsymbol{\lambda}_{v_f}] = \boldsymbol{\Phi}(t_f, t_0)[\delta\boldsymbol{r}_0; \delta\boldsymbol{v}_0; \delta\boldsymbol{\lambda}_{r_0}; \delta\boldsymbol{\lambda}_{v_0}] \tag{11}$$

Since the initial states are fixed, i.e., $\delta\boldsymbol{r}_0 = 0$ and $\delta\boldsymbol{v}_0 = 0$, the above expression simplifies accordingly. Moreover, because the costate is zero on the nominal trajectory, then $\delta\boldsymbol{\lambda} = \boldsymbol{\lambda}$ at all times.

Additionally, the variations of the final states are defined as, $\delta \boldsymbol{r}_f = \boldsymbol{r}_f - \boldsymbol{r}_p$ and $\delta \boldsymbol{v}_f = \boldsymbol{v}_f - \boldsymbol{v}_p$, where $\boldsymbol{r}_p$ and $\boldsymbol{v}_p$ represent the final nominal states obtained from the propagation of simple Keplerian motion over the time interval $[t_0 \ t_f]$. Consequently, the IVP reduces to solving a linear system of initial costate $(\boldsymbol{\lambda}_{r0}, \boldsymbol{\lambda}_{v0})$, which is presented as,

$$\begin{bmatrix} \boldsymbol{\lambda}_{r_0} \\ \boldsymbol{\lambda}_{v_0} \end{bmatrix} = (\boldsymbol{\Phi}_{\lambda_0})^{-1} \begin{bmatrix} \boldsymbol{r}_f - \boldsymbol{r}_p \\ \boldsymbol{v}_f - \boldsymbol{v}_p \end{bmatrix} \tag{12}$$

Here, $\boldsymbol{\Phi}_{\lambda_0}$ refers to the 6×6 submatrix in the upper right corner of $\boldsymbol{\Phi}(t_f, t_0)$, which connects $[\delta \boldsymbol{r}_f; \delta \boldsymbol{v}_f]$ and $[\delta \boldsymbol{\lambda}_{r_0}; \delta \boldsymbol{\lambda}_{v_0}]$, i.e., $\boldsymbol{\Phi}_{\lambda_0} = \boldsymbol{\Phi}(t_f, t_0)[1 : 6, 7 : 12]$. It should be noted that the matrix $\boldsymbol{\Phi}_{\lambda_0}$ may be non-invertible for certain thrust directions, rendering the associated linear system unsolvable. To mitigate this issue, least-square solutions are adopted in solving the linear system Eq. (12). For each direction, this least-square solution yields an energy-optimal control law that minimizes the deviation between the desired and the controlled final state, thereby enabling a robust estimation of control when an exact solution is not attainable. $[\boldsymbol{r}_p; \boldsymbol{v}_p]$ are calculated analytically using Keplerian motion, and the same analytical approach is applied to propagate the leader's orbital state. Although mission requirements for relative hovering are typically defined in terms of relative states, once the target relative state and control duration are specified, the follower's target inertial state $[\boldsymbol{r}_f; \boldsymbol{v}_f]$ can easily be derived from the leader's final inertial state based on the definition of the LVLH frame.[22]

For each constant thrust direction defined by angles α and β, a least-square solution to the corresponding energy-optimal control problem is obtained by solving Eq.(12). This process requires only a single integration of Eq.(9) for each direction, alongside the integration of simple Keplerian dynamics. To assess and select the most favorable direction based on control performance, an additional integration of Eq. (7) is carried out using the derived initial costate. This enables the evaluation of key performance metrics such as fuel consumption and the final state error relative to the desired target. The reliability of these least-square energy-optimal solutions in identifying an effective thrust direction is validated in the numerical simulations part through comparisons with high-fidelity numerical solutions obtained using the shooting method.

Fuel Optimal Control

With an initial guess for the thrust direction and nominal firing window derived from the energy-optimal solutions, the fuel-optimal control problem can be efficiently solved using a nonlinear programming approach. An overview of this procedure is illustrated in Figure 2.

Given a maximum acceleration magnitude $a_{\max}$, a nominal firing window is extracted from the energy-optimal solution using a bisection method, similar to the approach in References 20, 21. In the fuel-optimal control problem, the thrust direction defined by the constant angles α and β is also treated as an optimization variable. The initial guess for these angles is selected based on the energy-optimal solutions, typically by choosing the direction that exhibits the best performance within the explored domain. With both the selected thrust direction and its associated nominal firing window, a NLP problem is formulated to determine a feasible solution. The objective is to identify an optimal bang-bang control profile and thrust direction that minimize fuel consumption approximated by total firing time, while satisfying mission constraints. If a feasible solution cannot be obtained using the best-performing direction as the initial guess, neighboring directions are explored as alternative starting points.

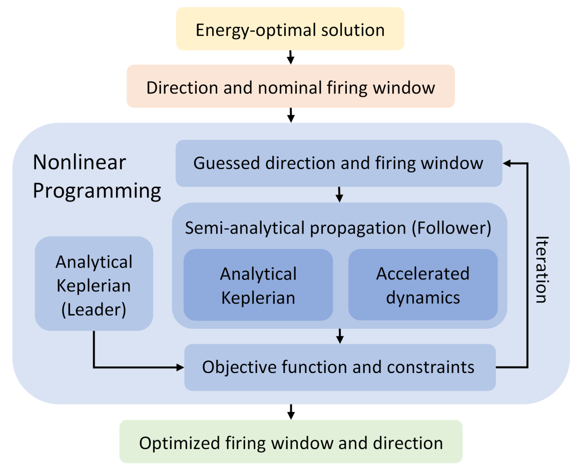

Figure 2. Procedure for fuel optimal solution.

In the NLP formulation for this problem, there are no equality constraints. However, two inequality constraints are imposed on the magnitudes of final relative position and velocity,

$$\begin{aligned} X_{r_f} &\leq X_{r_e} \\ X_{v_f} &\leq X_{v_e} \end{aligned} \tag{13}$$

Here, X_{r_f} and X_{v_f} are the magnitudes of the controlled final relative position and velocity vectors, and X_{r_e} and X_{v_e} represent the required accuracies, set to 0.1 m and 0.001 $\mathrm{m/s}$, respectively. An extra inequality constraint is introduced based on the final periodicity condition, whose definition can be found in Reference 20,

$$p_1 x(t_f) + p_2 \dot{x}(t_f) + p_3 z(t_f) + p_4 \dot{z}(t_f) \leq P_e \tag{14}$$

where $p_i, i = 1, 2, 3, 4$ are parameters calculated from the final inertial state of the leader and P_e is a threshold, set to 10^{-3} which is consistent with the value adopted in Reference 20.

For solving this NLP, the optimal bang-bang thrust structure is determined by adjusting the durations of thrusting arcs within the nominal firing window. Specifically, the centers of the thrusting arcs are fixed, while their durations can be extended or shortened. A constraint is enforced to prevent overlapping between adjacent arcs. As a result, the number of thrusting arcs cannot increase, but may decrease if any thrusting arc reduces to zero. The objective function is minimized iteratively by adjusting both the thrust direction and the durations of the thrusting arcs. For each iteration, forward state propagation is performed to evaluate constraint satisfaction. The nonlinear inertial dynamics model used in the energy-optimal problem is directly adopted, enabling application to general orbits. Since the state propagation involves both the follower and the leader, their trajectories are computed separately but over the same total time. For the follower's thrusting arcs, numerical integration of the accelerated inertial dynamics is carried out, given the specified magnitude and RTN-constant thrust direction. For the coasting arcs of the follower and the full trajectory of the leader, which follow Keplerian motion, analytical propagation is used for computational efficiency. In the following section, the validation of this procedure to obtain fuel-optimal solution is verified by numerical simulations.

NUMERICAL SIMULATIONS

The strategy to perform long-term hovering control was developed in Reference 20. The key idea is to apply control actions only when the follower spacecraft exits a predefined hovering region due to orbital perturbations, such as the J_2 effect and atmospheric drag. This strategy divides operations into two main phases: a drifting phase, also referred to as the hovering phase, and a control phase. The drifting phase involves uncontrolled relative motion within the hovering region. The follower begins this phase from a point on a predefined naturally periodic relative orbit. As perturbations accumulate, the relative motion gradually deviates from this orbit until it reaches the boundary of the hovering region, and the intersection point serves as the initial condition for the subsequent control phase. The objective of the control phase is to guide the relative motion from this initial state back to a target state on the reference periodic relative orbit. Together, these two phases form one hovering control cycle. Long-term hovering is then achieved through the repetition of multiple such cycles. This study focuses on simulating a single hovering control cycle.

Table 1. Parameters of simulation

Parameters	Value
Gravitational parameter of Earth	$\mu = 3.986004 \times 10^5 \mathrm{km}^3/\mathrm{s}^2$
Radius of the Earth	$R_e = 6.378136 \times 10^3 \mathrm{km}$
J_2 parameter	1.08263×10^{-3}
Ballistic coefficients	$B_l = 150.30 \mathrm{kg/m}^2$,$B_f = 153.40 \mathrm{kg/m}^2$
Initial orbital elements of leader	$P = 450 \mathrm{km}$, $e = 0.01$, $i = 30°$, $\Omega = 0$, $\omega = 0$, $\nu = 0$

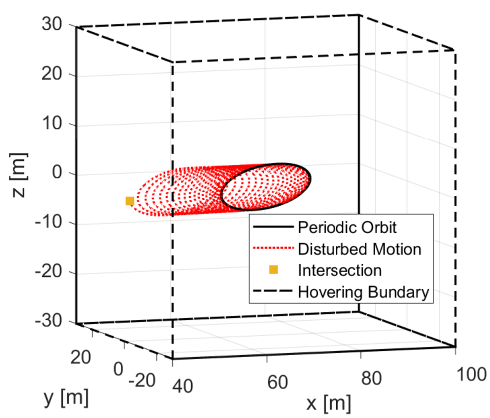

Figure 3. Drifting phase of relative hovering.

The Simulink model of Reference 24 is adopted as a ground truth dynamical model which is based on the nonlinear Gauss variational equations including Earth J_2 oblateness effect and atmospheric drag as perturbation sources. The simulation parameters are summarized in Table 1. The two spacecrafts are considered to be similar, where the values of the follower have been directly taken from Reference 24. This ballistic coefficient represents an average value between the ISS and the ATV as taken from Reference 17. The initial classical orbital elements of the leader are a perigee altitude of $P = 450\mathrm{km}$, an eccentricity of $e = 0.01$, and an inclination of $i = 30°$ while the rest of the elements are set to 0.[17,20] The hovering zone is defined as a cube along the positive $\boldsymbol{i}$ direction of the LVLH frame, and it can be defined by upper (overline) and lower (underline) bounds, $\{\underline{x} = 40\text{m}, \overline{x} = 100\text{m}, \underline{y} = -30\text{m}, \overline{y} = 30\text{m}, \underline{z} = -30\text{m}, \overline{z} = 30\text{m}\}$.[16,17,20] A target periodic orbit is solved from the Algorithm in Reference 20, where the y and z boundaries of the periodic orbit are set at 5 m, and the expected x-center is set as 70 m which is the center of the hovering zone. A simulation of the drifting phase is shown in Fig. 3, where the disturbed relative motion evolves from this natural periodic orbit to the boundary of the hovering zone.

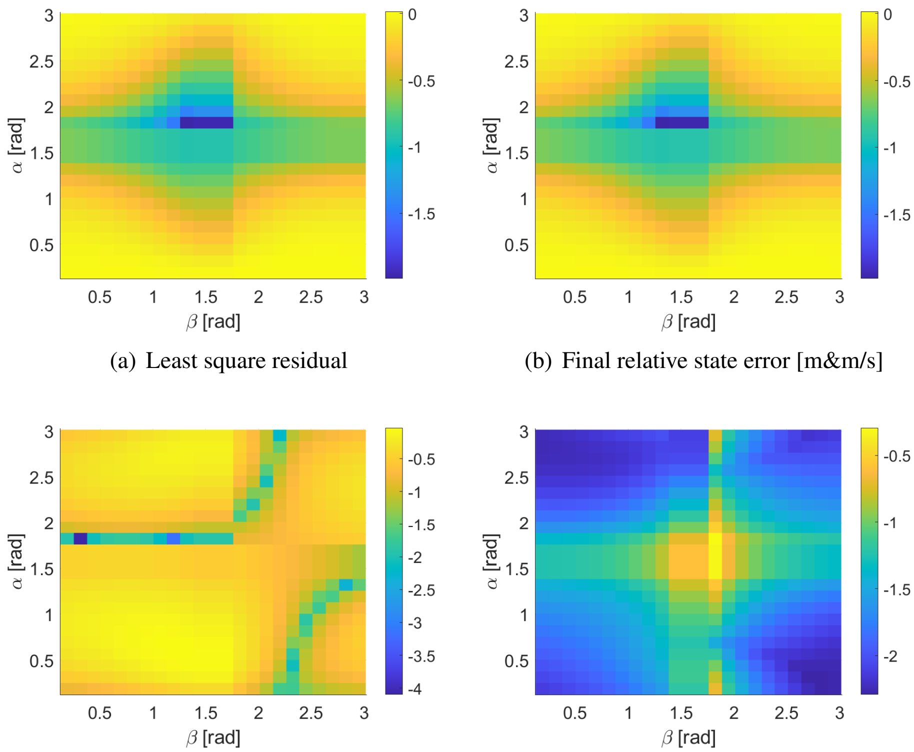

(a) Least square residual (b) Final relative state error [m&m/s]

(c) Final periodicity (d) Δv [m/s]

Figure 4. Energy optimal results in the given angle domain ($\log_{10}$)**.**

The energy-optimal solution is first simulated applying RTN-constant control direction. The control direction is characterized by two angles in the range of $\alpha \& \beta \in (0, 0.5\pi) \cup (0.5\pi, \pi)$. To apply the developed STM-based method, α and β are treated as known constants. When $\alpha = 0$ or π, the thrust direction lies entirely within the orbital plane, allowing only in-plane motion to be controlled. When $\alpha = 0.5\pi$, the thrust is aligned with the normal direction, enabling manipulation of only the out-of-plane motion. Additionally, $\beta = 0$ or π corresponds to tangential thrust within the orbital plane, while $\beta = 0.5\pi$ corresponds to radial thrust. In the following simulations, values of α and β near these critical angles are omitted to avoid redundant computations and reduce potential numerical integration errors. Here, these angles are selected as discrete points evenly spaced within the above range. Given a step size of $d\pi$ radians, the number of discrete points is $N = \lfloor 1/d \rfloor - 2$, where $\lfloor \cdot \rfloor$ denotes the floor function. This results in a total of $N \times N$ constant directions, requiring the solution of $N \times N$ energy-optimal problems to identify promising candidate directions suitable to initialize the fuel-optimal problem. As the number of discrete points N increases, the computational burden of solving all energy-optimal problems also increases. However, the Least-Square (LS) solutions can be obtained efficiently using the introduced analytical STM method. To evaluate the effectiveness of the LS solutions as reliable initial guesses, their performance is compared with results from numerical methods, including Indirect Shooting using a zero vector as the initial guess (IS-0) and Indirect Shooting using the LS solution as the initial guess (IS-LS). All LS and indirect shooting solutions are implemented in MATLAB using the *fsolve* function with the *Levenberg–Marquardt* algorithm.

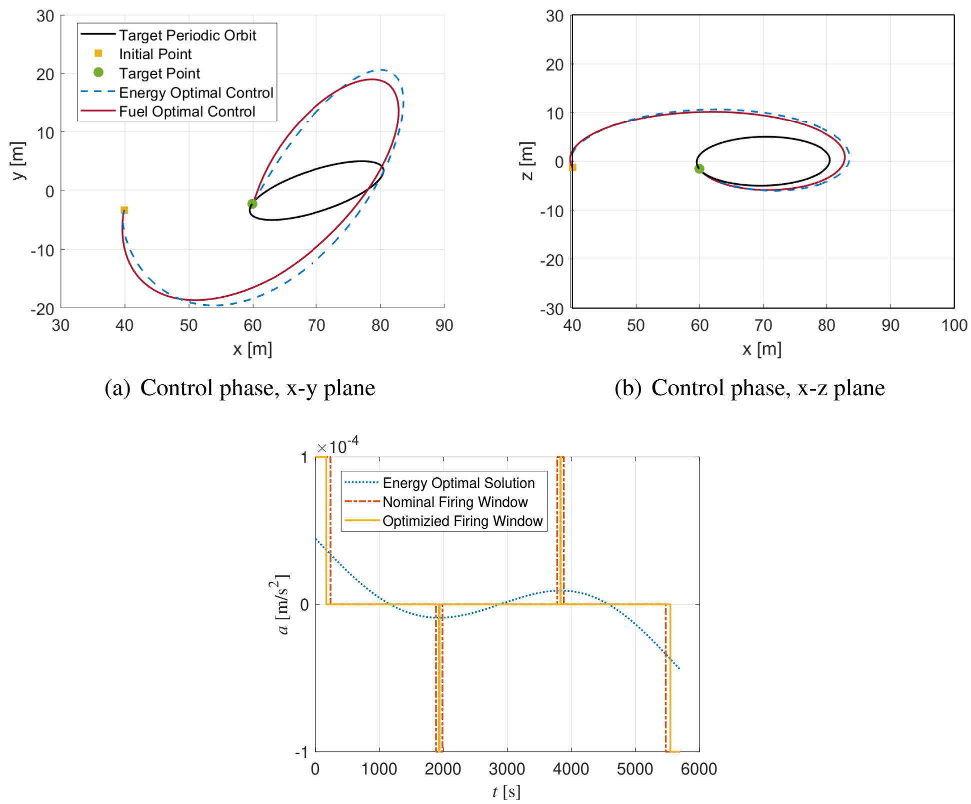

(a) Control phase, x-y plane

(b) Control phase, x-z plane

(c) Acceleration profile

Figure 5. Simulation results of optimal control.

A simulation is performed to demonstrate the proposed control method. Initial state is the intersection of the drifting phase in Fig. 3, and the target point is determined by setting the control duration as one leader's orbital period.[20] The step difference is set to $d\pi = 0.05\pi$ radians, resulting in 18×18 (i.e., 324) directions being evaluated. For the given control mission with this set of constant directions, the least square solutions are fast computed. The results are presented in Figure 4, including the least square residual, final relative state error, final periodicity condition, and fuel cost (ΔV). These results are also compared with those obtained by a numerical indirect shooting method. As the distributions and values of the results are virtually identical in LS, IS-0, and IS-LS methods, they are collectively represented in Fig. 4. It is found that the results of least square solutions are nearly the same as the numerical results. Therefore, selecting beneficial constant thrust directions based on the least square approach is shown to be a reliable and efficient strategy. The final periodicity condition is calculated based on the final in-plane relative states using Eq. (14). This condition is a fundamental requirement for enabling long-term hovering by initializing a naturally periodic relative motion at the end of the control phase. Furthermore, a comparison between the final relative state error obtained from the LS solution and the corresponding least square residual indicates that the LS method introduces negligible errors in this small relative state change scenario.

Based on the final relative state error, periodicity condition, and fuel cost obtained from the energy-optimal solutions, a candidate constant thrust direction can be selected. This direction, along with the corresponding nominal firing window, serves as the initial guess for computing the fuel-optimal solution. The simulation results for the control phase using both the energy-optimal and the fuel-optimal strategies are presented in Figure 5. Figures 5(a) and 5(b) show the controlled relative trajectories, while Figure 5(c) illustrates the corresponding acceleration profiles, computed with a maximum acceleration magnitude of $a_{\max} = 1 \times 10^{-4}$ m/s^2. These results validate the effectiveness of the proposed RTN-constant low-thrust control strategy for achieving fuel-efficient and precise relative hovering.

CONCLUSION

This paper studies optimal low-thrust control strategies employing constant thrust directions defined in the local Radial-Transverse-Normal frame. Unlike control schemes constrained to specific directions, such as tangential-only thrust, the proposed RTN-constant control strategy enables full six-degree-of-freedom orbital control, making it suitable for a wider range of mission scenarios. Computationally efficient methods are developed to solve both energy-optimal and fuel-optimal problems while identifying favorable constant thrust directions. The effectiveness of the proposed approach is demonstrated through a relative hovering mission scenario. The energy-optimal problem is addressed analytically using an inertial state transition matrix approach, which provides least-square solutions. Numerical simulations confirm that these solutions effectively identify promising candidate thrust directions, achieving reliable performance with significantly reduced computational cost compared to fully numerical methods. Moreover, the least-square approach maintains high accuracy in scenarios involving small relative state variations. Building upon the initial guesses for both thrust direction and nominal firing window, the fuel-optimal solution is obtained via nonlinear programming, utilizing semi-analytical forward state propagation. This integrated framework, combining analytical and numerical techniques, ensures both computational efficiency and high solution accuracy. Overall, the RTN-constant control strategy offers a robust and efficient solution for spacecraft relative hovering and shows strong potential for application in future low-thrust mission planning.

REFERENCES

[1] W. Fehse, *Automated Rendezvous and Docking of Spacecraft*. Cambridge, England, U.K.: Cambridge University Press, 2003, 10.1017/CBO9780511543388.

[2] M. Maestrini and P. Di Lizia, “Guidance Strategy for Autonomous Inspection of Unknown Non-Cooperative Resident Space Objects,” *Journal of Guidance, Control, and Dynamics*, Vol. 45, No. 6, 2022, pp. 1126–1136, 10.2514/1.G006126.

[3] M. Maestrini and S. Carcano, “Polynomial guidance laws for robust fuel optimal station-keeping of geostationary satellites,” *Acta Astronautica*, Vol. 236, 2025, pp. 173–187, https://doi.org/10.1016/j.actaastro.2025.06.047.

[4] M. Kobilarov and S. Pellegrino, “Trajectory Planning for CubeSat Short-Time-Scale Proximity Operations,” *Journal of Guidance, Control, and Dynamics*, Vol. 37, Mar. 2014, pp. 566–579, 10.2514/1.60289.

[5] C. Petersen, S. Phillips, K. Hobbs, and K. Lang, “Challenge Problem: Assured Satellite Proximity Operations,” *Proceedings of 31st AAS/AIAA Spaceflight Mechanics Meeting*, 2021.

[6] Z. Dang, Z. Wang, and Y. Zhang, “Modeling and Analysis of Relative Hovering Control for Spacecraft,” *Journal of Guidance, Control, and Dynamics*, Vol. 37, No. 11, 2014, pp. 1091–1102, 10.2514/1.G000004.

[7] N. Faraco, M. Maestrini, and P. Di Lizia, "Instance Segmentation for Feature Recognition on Noncooperative Resident Space Objects," *Journal of Spacecraft and Rockets*, Vol. 59, No. 6, 2022, pp. 2160–2174, 10.2514/1.A35260.

[8] M. Maestrini, M. A. De Luca, and P. Di Lizia, "Relative Navigation Strategy About Unknown and Uncooperative Targets," *Journal of Guidance, Control, and Dynamics*, Vol. 46, No. 9, 2023, pp. 1708–1725, 10.2514/1.G007337.

[9] P. R. Arantes Gilz, *Embedded and validated control algorithms for the spacecraft rendezvous*. PhD thesis, Université Paul Sabatier-Toulouse III, Toulouse, France, Oct. 2018.

[10] D. J. Scheeres, "Close Proximity Operations at Small Bodies: Orbiting, Hovering, and Hopping," *Mitigation of Hazardous Comets and Asteroids*, pp. 313–336, Cambridge University Press, 2004, 10.1017/CBO9780511525049.016.

[11] S. B. Broschart and D. J. Scheeres, "Control of Hovering Spacecraft Near Small Bodies: Application to Asteroid 25143 Itokawa," *Journal of Guidance, Control, and Dynamics*, Vol. 28, No. 2, 2005, pp. 343–354, 10.2514/1.3890.

[12] H. Xu, Y. Ye, and Z. Yang, "Nonlinear Control of Underactuated Spacecraft Hovering," *Journal of Guidance, Control, and Dynamics*, Vol. 39, No. 3, 2016, pp. 685–694, 10.2514/1.G001306.

[13] D. J. Irvin, R. G. Cobb, and T. A. Lovell, "Fuel-Optimal Maneuvers for Constrained Relative Satellite Orbits," *Journal of Guidance, Control,and Dynamics*, Vol. 32, No. 3, 2009, pp. 960–973, 10.2514/1.36618.

[14] G. Deaconu, C. Louembet, and A. Théron, "Designing Continuously Constrained Spacecraft Relative Trajectories for Proximity Operations," *Journal of Guidance, Control,and Dynamics*, Vol. 38, No. 7, 2015, pp. 1208–1217, 10.2514/1.G000283.

[15] P. R. Arantes Gilz, M. Joldes, C. Louembet, and F. Camps, "Model Predictive Control for Rendezvous Hovering Phases Based on a Novel Description of Constrained Trajectories," *IFAC-PapersOnLine*, Vol. 50, July 2017, pp. 7229–7234, 10.1016/j.ifacol.2017.08.1367.

[16] P. R. Arantes Gilz, M. Joldes, C. Louembet, and F. Camps, "Stable Model Predictive Strategy for Rendezvous Hovering Phases Allowing for Control Saturation," *Journal of Guidance, Control,and Dynamics*, Vol. 42, No. 8, 2019, pp. 1658–1675, 10.2514/1.G003558.

[17] J. C. Sanchez, C. Louembet, F. Gavilan, and R. Vazquez, "Event-Based Impulsive Control for Spacecraft Rendezvous Hovering Phases," *Journal of Guidance, Control, and Dynamics*, Vol. 44, No. 10, 2021, pp. 1794–1810, 10.2514/1.G005507.

[18] M. Maestrini, P. Di Lizia, and F. Topputo, "Analytical Impulsive-to-Continuous Thrust Conversion in Linearized Relative Dynamics," *Journal of Guidance, Control, and Dynamics*, Vol. 44, No. 4, 2021, pp. 862–871, 10.2514/1.G005520.

[19] M. D. Rayman, P. Varghese, D. H. Lehman, and L. L. Livesay, "Results from the Deep Space 1 Technology Validation Mission," *Acta Astronautica*, Vol. 47, No. 2–9, 2000, pp. 475–487, 10.1016/S0094-5765(00)00087-4.

[20] C. Zhao, M. Maestrini, and P. Di Lizia, "Low-Thrust Optimal Control of Spacecraft Hovering for Proximity Operations," *Journal of Guidance, Control, and Dynamics*, Vol. 47, No. 7, 2024, pp. 1457–1469, 10.2514/1.G008063.

[21] A. De Vittori, M. F. Palermo, P. Di Lizia, and R. Armellin, "Low-Thrust Collision Avoidance Maneuver Optimization," *Journal of Guidance, Control, and Dynamics*, Vol. 45, No. 10, 2022, pp. 1–15, 10.2514/1.G006630.

[22] Z. Dang, "New State Transition Matrix for Relative Motion on an Arbitrary Keplerian Orbit," *Journal of Guidance, Control, and Dynamics*, Vol. 40, No. 11, 2017, pp. 2917–2927, 10.2514/1.G002723.

[23] A. Bryson, *Applied Optimal Control: Optimization, Estimation and Control*. Boca Raton, FL: CRC Press, 2017.

[24] P. R. Arantes Gilz, "A Matlab®/Simulink® Non-Linear Simulator for Orbital Spacecraft Rendezvous Applications," https://hal.archives-ouvertes.fr/hal-01413328, 2016.